Computers & Graphics 33 (2009) 554–565

Contents lists available at ScienceDirect

Computers & Graphics

journal homepage: www.elsevier.com/locate/cag

Technical Section

Visual computing for medical diagnosis and treatment

Jan Klein [a,*], Ola Friman [a], Markus Hadwiger [b], Bernhard Preim [c], Felix Ritter [a], Anna Vilanova [d], Gabriel Zachmann [e], Dirk Bartz [f]

[a] Fraunhofer MEVIS – Institute for Medical Image Computing, Germany
[b] VRVis Research Center, Vienna, Austria
[c] Otto-von-Guericke-University, Institute for Simulation and Graphics, Germany
[d] Eindhoven University of Technology, Department of Biomedical Engineering, The Netherlands
[e] TU Clausthal, Department of Informatics, Germany
[f] University of Leipzig, ICCAS (Visual Computing), Germany

ARTICLE INFO

Article history:
Received 1 September 2008
Received in revised form
9 April 2009
Accepted 28 April 2009

Keywords:
Medical visualization
Volume rendering
Diffusion tensor imaging
Vessel visualization
Image-guided surgery
Intra-operative imaging
Virtual and mixed reality
Occlusion handling
Collision detection

ABSTRACT

Diagnostic algorithms and efficient visualization techniques are of major importance for preoperative decisions, intra-operative imaging and image-guided surgery. Complex diagnostic decisions are characterized by a high information flow and fast decisions, requiring efficient and intuitive presentation of complex medical data and precision in the visualization. For intra-operative medical treatment, the pre-operative visualization results of the diagnostic systems have to be transferred to the patient on the operation room table. Via augmented reality, additional information of the hidden regions can be displayed virtually. This state-of-the-art report summarizes visual computing algorithms for medical diagnosis and treatment. After starting with direct volume rendering and tagged volume rendering as general techniques for visualizing anatomical structures, we go into more detail by focusing on the visualization of tissue and vessel structures. Afterwards, algorithms and techniques that are used for medical treatment in the context of image-guided surgery, intra-operative imaging and augmented reality are discussed and reviewed.

1. Introduction

Modern medicine produces large datasets with a strong annual rate of growth due to the development and the increasing differentiation of methods for medical diagnosis and treatment. Frequently, the sector of medical economics is seen as one of the central domains of innovation. At the same time, the number of medical doctors remains static, jobs have even been reduced at many sites, and the possibilities offered by medical technology are not fully utilized. This can be noticed especially in the area of medical image computing and the associated diagnosis and medical treatment. The employed techniques that acquire cross-sectional images may produce several thousand images within a few minutes and the trend is increasing. On the opposite of this technological potential, only few powerful and problem-adapted software systems and visualization tools exist so that a large part of the actual available image data remains unused.

A desired solution comprises the application of computer systems for supporting medical practice. Such software assistants for medical diagnosis and treatment are based on the idea that computers are able to do special issues reliably and efficiently while the diagnostic and therapeutic decision remains the task of medical experts. To implement an optimal collaboration and interaction between human and computer, software assistants have to be designed and tested for special tasks. Fundamental criteria are the robustness of technical and biological variations of the incoming data, a handling of measurement errors as well as efficiency and an acceptance of the software. For the latter point, visual computing algorithms for medical diagnosis and treatment play a decisive role as they constitute the most important interface between the software and the doctors.

This paper summarizes selected visual computing methods and processing algorithms for medical diagnosis (Section 3) and reviews algorithms which are used for medical treatment in the context of image-guided surgery, intra-operative imaging and augmented reality (Section 4). Advantages and disadvantages of the methods as well as directions for future work are shown.

We begin with volume rendering algorithms (Section 3.1), which constitute the basis for medical diagnostic visualization

* Corresponding author.
E-mail address: jan.klein@mevis.fraunhofer.de (J. Klein).

0097-8493/$ - see front matter © 2009 Elsevier Ltd. All rights reserved.
doi:10.1016/j.cag.2009.04.006

Table 1
A general overview of the presented techniques in our state-of-the-art report is given.

Clinical task	Algorithm/technique	Section
Image acquisition	CT, MRI, US	2
Visualization of scans in their entirety	Direct volume rendering	3.1
Multi-modality rendering, segmentation of different tissues or organs	Tagged volume rendering	3.1
Visualization of fibrous tissue	Fiber tracking	3.2
Grouping of anatomically similar structures	Clustering	3.2
Visualization of vessels	Model-based reconstruction, implicit visualization	3.3
Associate preoperative data with patient in operation room	Tracking, registration algorithms, intra-operative imaging	4.1, 4.2
Medical simulations, training	Virtual and mixed reality	4.3, 4.4, 4.5

systems. They offer overview presentations of scalar volumetric data from computed tomography (CT) or MR scans without prior segmentation of specific regions, organs or risk structures. In the context of volume rendering we consider the problem of interactive performance with very large medical data volumes as well as the problem of finding an appropriate transfer function that maps the scalar data values to optical properties.

Afterwards, the visualization of highly patient-specific, complex topology which are important risk structures for assessing operability is discussed. First, the visualization of fibrous tissue from complex tensor data will be explained (Section 3.2). The presented techniques range from simplification to scalar information, glyph visualization and the so-called fiber tracking. In addition, we also review fiber clustering methods that aim to extract structures with higher semantic meaning than a fiber or a tensor. Second, the reconstruction of vascular systems from scalar data is considered as an example (Section 3.3). In this context we focus on modeling to convey shape and topology.

In the second part of this paper we discuss and review algorithms and techniques that are used for medical treatment in the context of image-guided surgery, intra-operative imaging and augmented reality. The major issue here is how to associate the pre-operative datasets and diagnostic results (e.g., risk structures) with the patient on the operation table. We consider registration techniques, passive optical tracking, and electromagnetic field tracking, which have become more popular in the last few years (Section 4.1) as well as intra-operative imaging techniques (Section 4.2). Virtual and augmented reality methods which add useful context information from the reality are reviewed (Section 4.3) and we pay special attention to the inherent occlusion handling problem (Section 4.4). Collision detection algorithms are an essential component in image-guided surgery as well as in virtual and mixed reality applications. An overview of the well-proven techniques and of very promising new directions in that area is given in Section 4.5.

A general overview of the algorithms and methods presented in this state-of-the-art report is given in Table 1.

2. Medical data

Surgical intervention planning and clinical diagnostic systems benefit from the large variety of imaging modalities and visualization tools currently available. Before focusing on the visualization of anatomical structures in the next section, we give a short introduction to the three main imaging techniques which are currently available.

Computed tomography: The computed tomography technology, which reconstructs 3D image volumes of tissue density from X-ray projections taken in different orientations, is developing rapidly. The current trend is to use multiple X-ray sources and to broaden the X-ray detectors so as to shorten acquisition time and improve image quality. With current CT scanners one can, for example, acquire high resolution image volumes covering the entire human heart with voxel sizes below 0.5 mm in less than 100 ms, which makes CT very valuable in emergency situations.

Magnetic resonance imaging: Magnetic resonance imaging (MRI) scanners, which use static and time-varying magnetic fields for generating 3D volumes, also evolve at a fast pace toward stronger magnetic fields and improved hardware. While not quite delivering the same image resolution as CT, MRI is able to generate anatomical images with excellent contrast between soft tissue types, for example, between white and gray matter in the brain. Moreover, the flexible MRI technique is increasingly being used to depict functional information, such as cortical activation with functional MRI; blood flow with phase-contrast MRI generating 3D + time velocity vector fields [1]; as well as specialized anatomical information such as fiber connections in the brain using diffusion tensor imaging (DTI) [2]. The main advantages of MRI are the high soft tissue contrast, the possibility to define oblique cut planes for the acquisition, and the fact that no ionizing radiation is used. In contrast to CT and ultrasound (US), MRI scanners and their operating costs are more expensive and the image acquisition process is longer.

Ultrasound imaging: The third major imaging modality is ultrasound, which uses echoes of high frequency sound waves to generate images. The main advantages of ultrasound are the small and cost-effective hardware and the real-time image acquisition rate which is an advantage for intra-operative solutions. Also the ultrasound technology is evolving toward 3D image acquisition. However, the quality and the resolution is generally not as good as in CT and MRI.

3. Visualization of anatomical structures

In computer-assisted medical diagnosis and treatment, the visualization of anatomical structures plays an important role. In this section, we describe visualization techniques that can be used for displaying overview representations as well as specific organs or tissue. We begin with volume rendering as a general method, followed by the visualization of tissue data by diffusion tensor imaging. Finally, we depict a very special problem, namely the visualization of vessels, in order to give an example for the visualization of highly patient-specific, complex topology.

3.1. Volume rendering

Direct volume rendering (DVR) is the most common way of depicting scalar volumetric data such as CT or MR scans in their entirety, as opposed to extracting surfaces of objects of interest (e.g., bones, vessels), or looking at a series of individual slice images, which is still common in radiology. In contrast to viewing 2D slice images, looking at the whole 3D volume makes it considerably easier to perceive depth relations and follow structures that are not parallel to one of the image planes. An important example is the use of pre-operative planning in neurosurgery, where it is much more natural and accurate to plan the best and minimally invasive approach to a tumor in 3D. Another example where 3D visualization is essential is virtual endoscopy [3,4].

For brevity, we review the basics of volume rendering and the most common practical approaches only briefly. For more details, we refer readers to the literature [6]. Essentially, in DVR the image volume is thought of as a collection of particles with certain physical properties that describe their interaction with light, e.g., absorption, emission, and scattering of light, which are subsumed in an *optical model*. To obtain an image of the entire volume, the *volume rendering integral* corresponding to a chosen optical model is solved along rays from the eye point through pixels of the output image plane. This integral is solved via discretization, where individual samples are taken, mapped to optical properties, and composited in order to obtain an approximate result of sufficient quality.

In the medical context, interactive performance is crucial, and the most common state-of-the-art method is to perform ray-casting on the GPU (graphics processing unit) [7–10]. Earlier GPU-based methods were based on texture slicing [11]. Alternative approaches are CPU-based ray-casting [12], using dedicated hardware such as the VolumePro [13], shear-warp [14], or splatting [15]. The latter is especially suited to visualize sparsely populated volumes such as vasculature [16].

A fundamental practical problem of medical volume rendering has always been the significant size of volume data, which is usually tackled via bricking approaches [17]. Bricking can also be used in conjunction with single-pass ray-casting in order to remove the per-brick setup overhead [18]. Recent GPU ray-casting implementations employing bricking are able to render volumes with several thousand slices at interactive rates [10]. It is also possible to use out-of-core approaches to avoid loading the entire volume into CPU memory [19].

Current high-end GPUs are available with memory sizes from 512 MB to 4 GB, which enables rendering of relatively large volumes even without bricking. However, data sizes are growing constantly and it is important that the size of the volumes that can be rendered is not directly limited by the available amount of on-board memory. Naturally, memory requirements increase even further when multiple imaging modalities are visualized concurrently, or the data are time-dependent and thus consist of one or multiple volumes per time step.

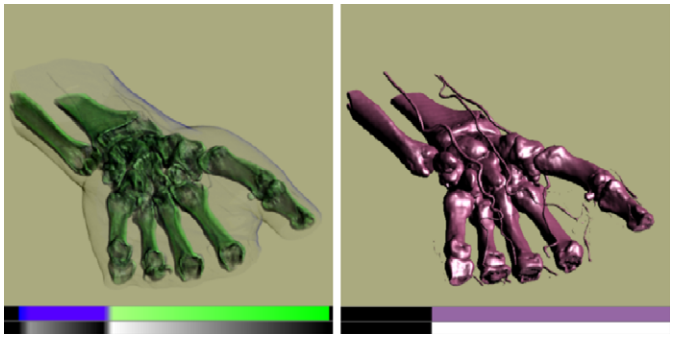

Fig. 1. In direct volume rendering (DVR), the *transfer function* maps the raw volume data to optical properties needed for image synthesis. Even a simple 1D transfer function allows for a lot of flexibility, from assigning varying amounts of transparency to certain structures (left), to essentially depicting isosurfaces without extracting geometry (right).

Interactive volume rendering has been restricted to orthogonal projection for a long time. However, recent advances in GPU-based ray-casting easily allow for perspective projections, which are especially important in virtual endoscopy [9] that focuses on the virtual representation of minimally invasive procedures for training, planning, and diagnosis without an actual invasive intervention. In contrast to texture slicing, ray-casting also increases flexibility, for example, allowing adaptive sampling rates [20]. In general, it is also easier to implement [6].

Incorporating ray-casting into an application for surgery planning and training provides more flexibility than extracting explicit geometry. For example, interactively changing the isovalue corresponding to the surface of the colon or a vessel in virtual endoscopy. For such applications, this can also include the display of segmented background objects [21], or the use of full DVR behind the surface [9].

Transfer functions: A major issue in DVR is how scalar data values are mapped to optical properties, which is commonly done via a global *transfer function*. In the simplest case, a transfer function is just a 1D table that maps density to color and opacity. Fig. 1 illustrates that this already enables a lot of flexibility, such as choosing from different semi-transparent depictions of multiple structures up to fully opaque results corresponding to isosurfaces. However, the specification of transfer functions is still a major hurdle for physicians, who are often overwhelmed by their complexity and the time required to specify them. Furthermore, many structures cannot be separated sufficiently with 1D transfer functions, and thus two or more dimensions are used [22,23].

Recent advances such as *semantic transfer functions* [5,24] can radically improve usability, and thereby increase the acceptance of volume rendering by medical doctors in the future. Fig. 2 shows visualizations generated using a semantic transfer function model that completely hides the underlying 2D transfer function domain from the user.

Another important issue is how to handle reliability or, vice versa, the *uncertainty*, which can be inherent in the visualization. A recent approach in the context of medical applications tackles this issue using probabilistic animation that results from applying a probabilistic transfer function [25], which is an approach to visually convey the uncertainty in a tissue classification task. Fig. 3 shows two frames from an animation sequence using this approach, where a probabilistic transfer function steers the animation. The amount of time that the boundary of a given structure is shown in a given color corresponds to the probability with which the boundary is actually located where it is shown in the visualization.

Both incorporating domain knowledge and domain-specific conventions and metaphors, e.g., semantic approaches, as well as visualizing error and uncertainty have been identified as important research challenges for the future by the NIH-NSF Visualization Research Challenges Report [26].

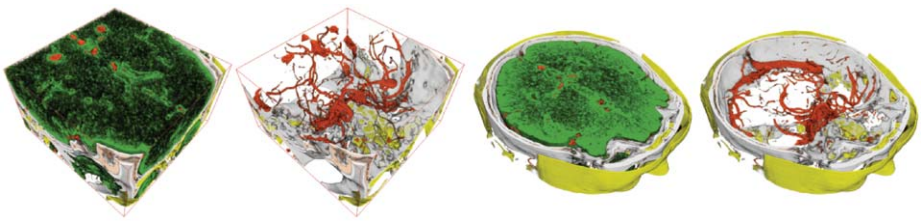

Fig. 2. Examples of a semantic transfer function model for CT angiography, with the anatomical structures brain, soft tissue, bone and vasculature [5]. Transfer functions are not specified directly, but via structures' names and visual attributes.

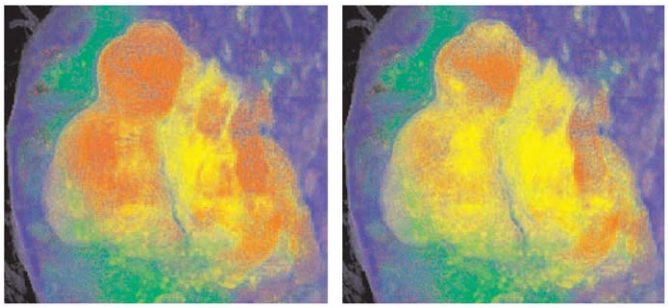

Fig. 3. Two frames of a real-time animation sequence that conveys the uncertainty regarding the border between a cyst and a hemorrhage in an MR brain examination [25].

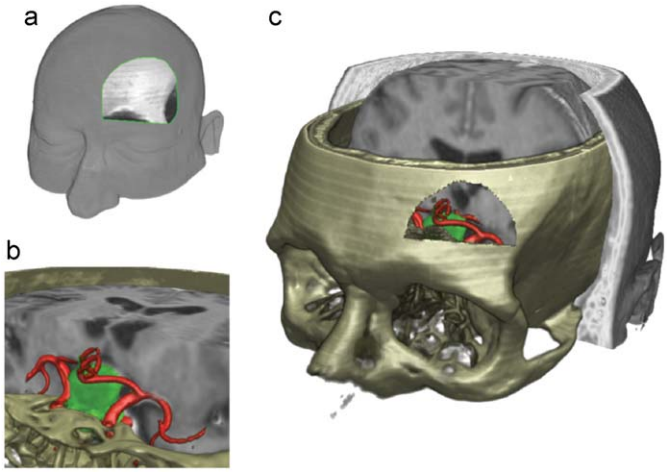

Fig. 4. Planning of a right subfrontal approach for pituitary tumor resection [28]. (a) Skin incision, (b) operating microscope view, and (c) keyhole approach planning. Single-pass ray-casting can combine multiple modalities in real-time: MRI (skin and brain); CT (bone); MRA (vessels).

Tagged volume rendering: If a transfer function alone does not suffice in order to separate different objects (tissues, organs) of interest, *segmentation* becomes necessary, which incorporates spatial information into the volume rendering process by specifying to which object each voxel belongs. Segmentation information can be used to define per-object transfer functions or rendering modes [27]. This makes it significantly easier to specify transfer functions and thus visually discriminate different anatomical structures, because optical properties can be assigned to each segmented structure individually. Segmentation also provides a powerful basis for multi-volume rendering in which multiple modalities such as CT, MRI, fMRI, and PET are combined on a per-object basis. In this case, transfer functions can be assigned individually to each segmented structure in each modality [28]. Fig. 4 shows three stages of an application for the preoperative planning of a neurosurgical keyhole approach. As in the specification of transfer functions, uncertainty is also a very important topic in segmentation. If a segmentation approach not only determines the binary masks for each segmented object, but also determines the uncertainty associated with the segmentation, this information can be included in the visualization as well [29].

One possibility to circumvent both, transfer function specification and segmentation, is to use *opacity peeling* [30]. This technique removes occluding parts of the volume in a view-dependent manner. However, opacity peeling can also be combined with the use of both transfer functions and segmentation, in order to combine their advantages. For example, opacity peeling achieves more accurate results when crucial structure boundaries are known or can be determined on-the-fly. An example of such an approach is *skull peeling* [28], where the structures occluding the brain in an MR volume are peeled away by using a co-registered CT volume to detect the structure boundaries of the skull. In this case, the CT data are used for on-the-fly thresholding of the bone, which is used to steer the peeling of the MR volume. The result is an unoccluded view of the brain.

3.2. Diffusion tensor imaging

Diffusion tensor imaging is a relatively new MR imaging modality that measures water diffusion in tissue [2]. The water molecules in tissue with an oriented structure, e.g., the white matter in the brain, tend to diffuse along these structures. The diffusion process is generally modeled by a Gaussian probability density function, or equivalently it is described by a second order tensor, i.e., a symmetric 3×3 matrix whose eigenvalues are real and positive. It is assumed that the diffusion tensor reflects the underlying tissue structure; for example, the main eigenvector points out the main orientation.

Applications: DTI was initially developed for visualizing white matter in the brain but its use has since been extended to include, for example, tumor dissection [31,32] and investigations of ischemic muscle tissue in the heart [33]. Specifically, after infarction the fiber structure of the heart muscle is remodeled to adapt to the new conditions. Changes in the fiber structure can be measured with DTI, with the aim of understanding why the fiber remodeling sometimes fails, leading to a collapse of the heart. Yet another interesting application is the use of DTI for preterm neonates or neonates who suffer from hypoxic ischemia [34] (a disorder characterized by a reduction in oxygen supply (hypoxia) combined with reduced blood flow (ischemia) to the brain). Being able to detect possible damages in the brain at an early stage yields the possibility to initiate a therapy that ensures the best possible development of the child. For all these applications, advanced visualization plays a crucial role, as the raw DTI data acquired by the MR scanner do not lend itself to visual inspection.

Visualizing DTI tensors: The most common DTI visualization technique used in clinical environments is based on a scalar valued function of the tensor, i.e., the information in the six independent variables of the 3×3 symmetric tensor is reduced to one scalar that represents some relevant characteristic, mainly the diffusion anisotropy which describes the direction preference of the diffusion process [35]. The resulting scalar data can be visualized using common scalar field visualization techniques; from 2D cutting plane color mappings to volume rendering or even surface information that may reveal anatomically relevant information [36].

When visualizing intrinsic 6D data as scalars, information is inevitably lost. In case of diffusion tensors, diffusion shape and orientation cannot be conveyed in maps of diffusion anisotropy. Another group of techniques use glyph representations to visualize the tensor data, see Fig. 5(i). Several glyph shapes have been used, e.g., ellipsoids, cuboids, and superquadrics [37]. These methods are able to show the full tensor data without any information reduction. However, the clinical value of this visualization technique remains an open question as a human may have difficulties perceiving relevant information. Although techniques have been proposed to improve the perception by optimizing the placement of glyphs [38], cluttering is still a problem.

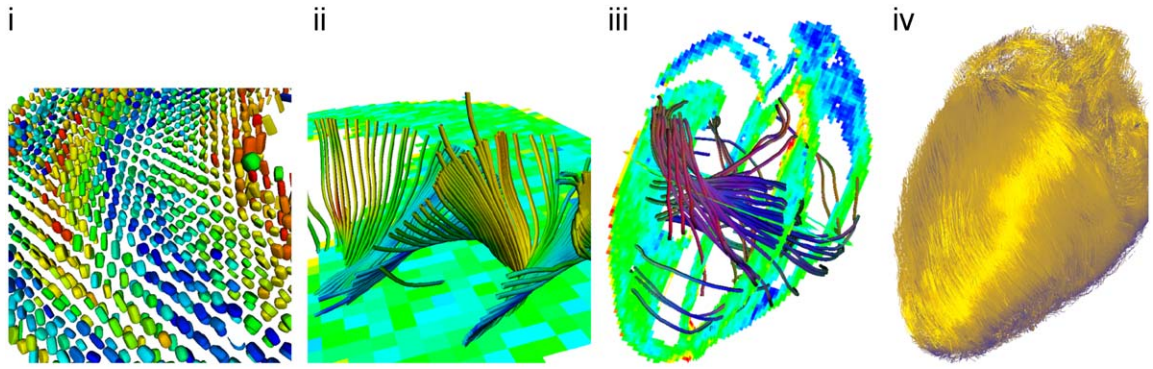

Fig. 5. Different visualizations of a healthy mouse heart dataset with resolution $128 \times 128 \times 64$: (i) superquadrics glyph in a region of the heart using hue color coding of the helix angle. (ii) Limited length fiber tracks obtained with seeding in a radial line. It shows the local helix form. (iii) Fiber tracking with region seeding. Fibers are shown as tubes and color coded according to main eigenvector. Cross sections showing hue color map of the fractional anisotropy. (iv) Fiber tracking with full volume seeding and using illuminated streamlines.

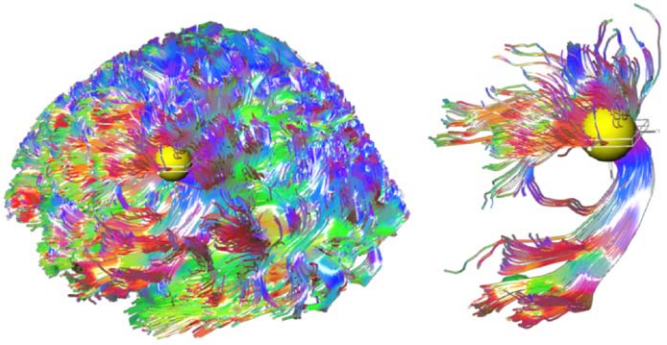

Fig. 6. Fiber tracking techniques determine the fibrous tissue structure from diffusion tensor information. Left: whole-brain fiber tracking result; right: fibers going through yellow sphere can be displayed in real-time.

Fig. 7. Brain connectivity maps generated by tracking a large number of traces from the points indicated by the arrows. Such maps can be used to delineate risk structures, in this case the corpus callosum in the brain. The white arrows indicate the seed points used for starting the tracking.

Fiber tracking: Fiber tracking techniques aim at reconstructing the fibrous tissue structure from the diffusion tensor information, see Fig. 6. The advantage of these methods is that the result is analogous to what the physicians or radiologists are expecting and an extensive amount of research has therefore been focused on this reconstruction [39–41]. Using streamline algorithms, the tensor field is reduced to a vector field consisting of the main eigenvectors of the tensors. This vector field can then be visualized using common techniques in flow visualization. An extension to streamlines are streamsurfaces, where a surface represented by the two main eigenvectors is reconstructed in areas of planar anisotropy [42,43]. The disadvantage of the streamline methods is that they do not make full use of tensor information, and thresholds based on anisotropy indices are required to define when the main eigenvector is valid. Another disadvantage is that the results are dependent on the seeding strategy for the streamlines. Often the seeding regions are defined subjectively by the user and relevant information can be missed with unfortunately chosen seed points.

Probabilistic tracking methods aim at visualizing the uncertainty present in DTI data by incorporating models of the acquisition process and noise [44–46]. The uncertainty is assessed by tracking many possible paths originating from a single seed point and in this process taking the tensor uncertainty into account. Based on the tracked paths, the maps of connectivity probabilities are produced, see Fig. 7. Such maps may be used to delineate risk structures for pre-surgical planning.

Fiber clustering: In practice, the interesting structures are not individual fibers, which in any case are impossible to reconstruct, since the DTI resolution is much lower than the diameter of the individual fibers. Instead, the interesting structures are anatomical meaningful bundles that are formed by fibers. Furthermore, it is interesting to compare individuals or groups of individuals, e.g., patients and normal controls, and quantify similarities and differences.

Fiber clustering algorithms [47–49] have been developed to group anatomically similar or related fibers into bundles (see Fig. 8(ii) and (iii)). As no user interaction is needed, undesirable bias is excluded. One of the main questions in several of these algorithms is to decide when the two fibers are to be considered similar or related, forming a bundle. Different distance/similarity measures between fibers are employed (e.g., Hausdorf distance, mean distance [49]).

3.3. Visualization of vessels

Knowing the branching pattern and topology of vascular structures is crucial for planning and performing surgery. 3D visualizations of vascular structures that convey the location, properties, spatial distances, and functional relationships of vessels to other relevant anatomic structures have been a frequent request by surgeons. Such visualizations should mainly work with CT images due to the better resolution compared to MR data. Ideally, the visualization should be static, yet providing all necessary morphological and spatial information in one single picture. The perception of spatial distances, however, becomes demanding when viewing a static, monoscopic projection of a 3D

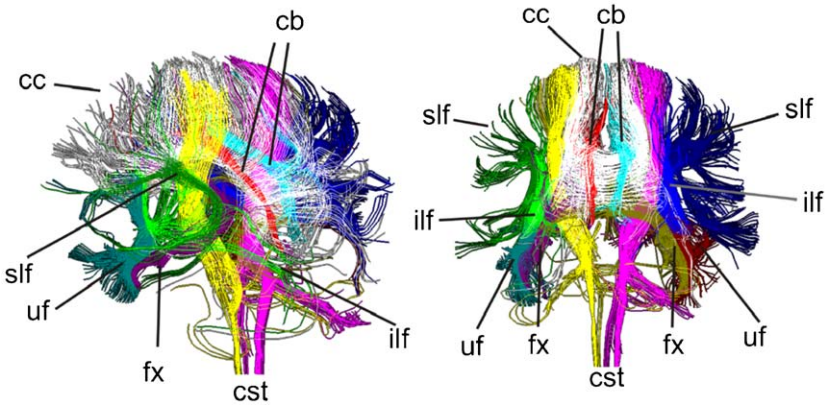

Fig. 8. The visualization of clustered fiber tracts improves the perception and allows for a better interaction with the data, e.g., single bundles can be selected for quantification processes (cc = corpus callosum, slf = superior longitudinal fasciculus, cb = cingulum bundle, ilf = inferior longitudinal fasciculus, cst = cortico-spinal tract, fx = fornix, uf = uncinate fasciculus).

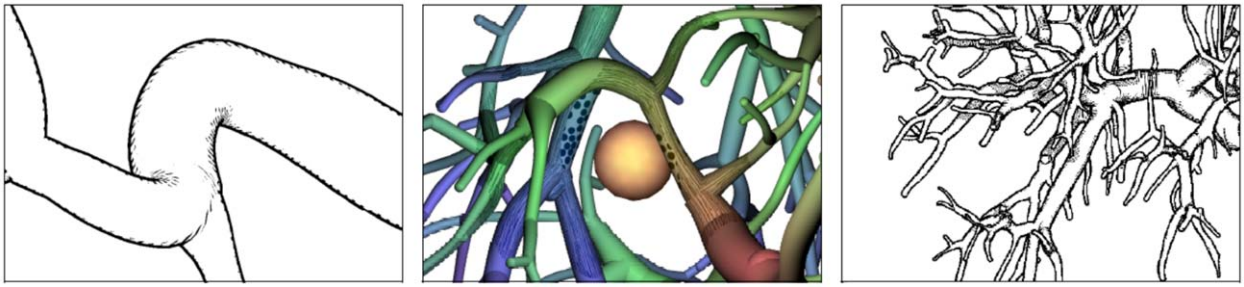

Fig. 9. Examples of vascular illustrations enhancing perception of properties important in surgery. Left and right image: hatching indicates curvature and distances; middle image: textures indicate distances to a lesion (orange).

visualization. This is especially true for complex vascular systems that may consist of multiple interweaved tree-like structures such as the vascular systems of the liver (portal vein, liver artery, hepatic veins, and biliary ducts). The effectiveness and lucidity of the visualization highly depend on the accentuation of spatial depth as well as the perceptive separation of important, individual properties. Algorithms aiming at improving spatial perception, particularly depth perception, and at communicating important vascular properties by using and extending illustrative visualization techniques have been proposed in Ritter et al. [50], see Fig. 9.

Conventional visualization techniques: For the diagnosis of vascular diseases, visualization techniques, such as direct volume rendering, maximum intensity projection and isosurface rendering, are employed. With these methods, the underlying image data are faithfully represented [51]. However, artifacts due to inhomogeneity of contrast agent distribution and aliasing problems due to the limited spatial resolution may hamper the interpretation of spatial relations. Direct volume rendering of segmented vascular structures is feasible and may be used to emphasize specific features of the vessel wall, such as plaques [52]. Therefore, explicit surface reconstructions of vascular structures are often preferred for surgical therapy planning and intra-operative visualization, where the interpretation of vascular connectivity and topology is more important than the visualization of vascular diseases [53].

Model-based reconstruction: The idea of model-based reconstruction aims at improving the reconstruction of vascular connectivity. Other reconstruction methods use the skeleton of a vascular tree and the local radius information as input. Assuming a circular cross section, surfaces of vascular trees are either explicitly constructed or created by means of an implicit description. Among the explicit methods, graphics primitives such as cylinders [54] and truncated cones [55] have been employed. These primitives are fitted along the cylinder and scaled according to the local diameter of vascular structures. Since skeletonization algorithms generally produce centerlines connecting voxel centers, the visual quality may be improved by smoothing the vessel skeleton, e.g., with a binomial filter [55]. A general problem of these methods is discontinuities at branching points. To overcome such problems, smooth transitions can be modeled by freeform surfaces [56]. The most advanced explicit reconstruction technique is based on subdivision surfaces [57]. An initial base mesh is constructed along the vessel centerline. The base mesh consists of quadrilateral patches and can be subdivided and refined according to the Catmull–Clark scheme.

Implicit visualization of vascular structures: Implicit modeling, as a special variant of model-based reconstruction, is used to obtain smooth shapes. A special variant, convolution surfaces, can be used to represent skeletal structures [58]. With careful selection of a convolution filter, this concept can accurately represent the local diameter of vascular structures [59]. The implicit surface description has to be polygonized, e.g., with a variant of Bloomenthal's polygonizer. The accuracy of this polygonization can be adjusted to either focus on speed or accuracy. In an evaluation with 12 medical doctors, it was shown that the improved visual quality improves the acceptance of 3D visualizations of vascular structures. A comprehensive survey of methods for vessel analysis and visualization can be found in Bühler et al. [60].

4. Visual computing for medical treatment and simulation

A classic vision in surgery is to provide the surgeon with an "X-ray view" with which interior regions of the body that are

hidden behind other organs are visualized. Virtual reality—or actually augmented or mixed reality—techniques are addressing this by enriching (“augmenting”) the view of the patient with virtual information of the hidden regions. Of particular interest are the regions or organs that are classified as risk structures, like vascular structures (Section 3.3) or white matter fiber tracts (Section 3.2), because they are vital and must not be damaged during the surgical intervention.

4.1. Image-guided surgery

Information of risk structures of interest can be acquired by a pre-operative scan of the patient, typically done with a CT or MRI scanner. While this is already a common practice in diagnosis and surgery planning (see Section 3.2), the major issue here is how to relate the pre-operative dataset(s) with the patient on the operation room (OR) table. The solution for this problem is to register the dataset to the patient, or actually the OR table to which the patient is fixed. This process requires the association of landmarks visible in the dataset and on the patient. While a minimum of four such associations is needed, typically six or more associations are established to improve accuracy and stability of the registration. Unfortunately, anatomical landmarks can vary significantly and are sometimes very difficult to identify. Instead, artificial markers, fiducials—which are easy to locate in the dataset and on the patient—are attached to the patient before the pre-operative scan.

After establishing the geometric transformation between the dataset and OR table, the virtual data from the dataset can be related to the patient, provided that the patient is not moved independently from the OR table.

Tracking: The position and orientation (or pose) of the OR table is measured based on a reference array—which is a defined, identifiable object—that in turn is measured by a tracking system. While a number of different methods are conceivable, passive or active optical tracking based on light sources and cameras is the current, most widely used technique. For passive tracking, one (or more) infrared light sources emit infrared light that is reflected by spherical markers of the reference array and again captured by two cameras mounted in a fixed geometric relationship. In contrast, active tracking uses several LED light sources that are directly identified by the cameras. While the former concept does not require an active control or energy supply, the latter requires batteries—which at latest need to be replaced after each intervention—and cable- or wireless-based control. In turn, the higher grade of control for active tracking allows more flexibility (active on/off switching of the LEDs) and hence somewhat better accuracy in certain situations. Once the markers have been identified, their positions are computed by triangulating the information of the image position of the marker by both cameras. To also compute the orientation of the reference array, a minimum of three markers in a constant geometric relationship is needed. Since the cameras measure projections of the markers, the accuracy of the computed position depends on the geometric arrangement of the markers; the further from linear dependence they are, the better.

Pointers, endoscopes, probes and other tools are tracked through another marker array (instrument array) by the tracking system, see Fig. 10. Different geometric configurations (number of markers, distance and angles between the markers) identify each tool.

Alternatively to optical tracking, electro-magnetic field tracking is also becoming increasingly popular. Electro-magnetic tracking has clear advantages, in that it does not require a static relationship between tooltip and reference markers and also does not need optical visibility of the markers. The disadvantage is that it is subject to various electro-magnetic field measuring artifacts, when ferromagnetic or metal objects are introduced into the magnetic field. More details can be found in Preim and Bartz [61].

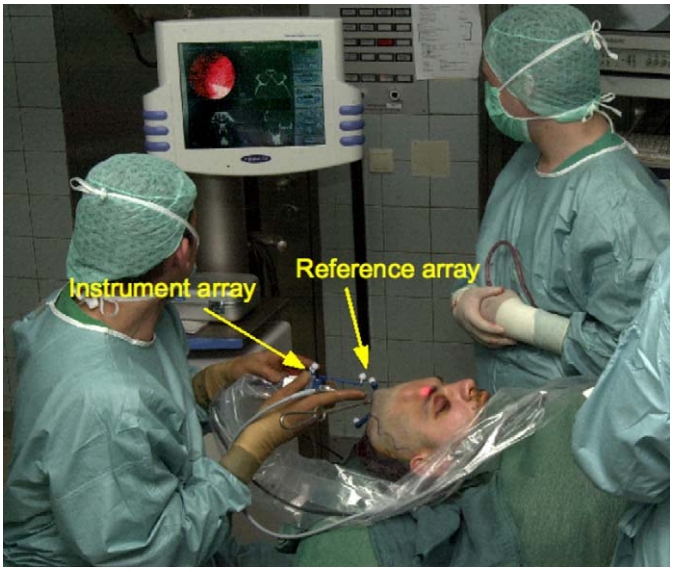

Fig. 10. Tracking of a surgical screw driver through an instrument array. Image is courtesy of Jürgen Hoffmann, Universität Tübingen.

In surgery, the combined system of marker/sensor arrays and tracking system is called an intra-operative navigation system and largely defines the field of image-guided surgery.

Unfortunately, a number of caveats come with the electro-magnetic tracking approach. First, the accuracy largely depends on the accuracy of the registration procedure. An inaccurate registration will lead to an insufficient overlap between dataset and patient. Second, several environmental factors may introduce measurement inaccuracies, which reduce the tracking quality. In particular optical tracking is sensitive to scattered infrared light from day light or physical deformations of the camera array during the warm-up. Finally, the whole procedure builds on the assumption that the patient has not changed significantly since the pre-operative scan. If this assumption is not sufficiently correct, the whole registration procedure becomes dramatically more complex, because the body changes induce deformations of the datasets, possibly down to every voxel. Therefore, this situation requires elastic (non-rigid) registration with computational costs that are currently prohibitive for the surgical routine.[1] An overview of different registration techniques (rigid and non-rigid), can be found in Maintz and Viergever [62].

4.2. Intra-operative imaging

An alternative to advanced registration approaches, intra-operative imaging re-scans the patient on the OR table. An example where this alternative is typically chosen is in brain surgery, where changes of pressure in the head after opening of the skull and of the dura (the leather-like hard skin of the brain) lead to position and shape changes of the brain. The so-called brain shift becomes even stronger after the (surgical) removal of tissue (e.g., tumor tissue) from the brain. The downside is that intra-operative scanning is a complex issue and typically requires a compromise on either image quality or costs. Intra-operative

[1] Next to the computational costs, elastic registration also gives rise to questions how accurately the details of a deformed dataset represents the reality.

scanners must generally be more mobile and less complex than pre-operative scanners or other restrictions apply which leads to a lower image quality. For example, intra-operative MRI scanners are used to provide access for the surgeons to the patient, hence the name open MR has been established [63]. Technical boundary conditions unfortunately only allow a weaker magnetic field, meaning a lower image quality. Recently, full field MRI scanners were introduced into the OR, providing an image quality comparable to regular pre-operative scanners [64]. Unfortunately, intra-operative full field MRI requires numerous changes to the OR, making it an expensive alternative.

Intra-operative ultrasound is well established and a cost-efficient scanning method, where a tracked ultrasound probe acquires 2D or 3D data in real-time. In many situations, it can be used as a valuable tool [65–68]. Alternatively, calibrated and tracked intra-operative X-ray systems are an option proposed by Navab et al. [69].

4.3. Virtual and mixed reality

Virtual reality simulates the interaction with virtual objects, which—as the name suggests—do not physically exist. With such medical simulations, surgeons can try out different approaches without exposing the patient to any risks. These simulations are adaptable to a wide range of clinical situations [70]. A specific virtual reality application in medicine is virtual endoscopy, where a virtual camera inspects body cavities in a representation acquired by a CT or MRI scanner, see Fig. 11. Since a previous survey report has already focused on virtual endoscopy [3], we just direct the interested user to that paper.

In contrast, virtual objects are added to a representation of reality in a mixed (augmented) reality system, whereas reality is captured either by an optical see-through display, e.g., a head-mounted display (HMD) [71,72] or a semi-transparent display [73], or by a video see-through display [74]. Optical see-through approaches represent the reality by direct viewing through (semi-)transparent glasses. Subsequently, the virtual objects are projected onto the glasses. While this approach has the advantage of no or little additional processing, it only provides a limited visual quality, since the reality is attenuated by the glass. In contrast, video see-through uses a camera to acquire the reality and embeds the virtual information in a post-processing step. This gives a better visual quality but higher processing costs.

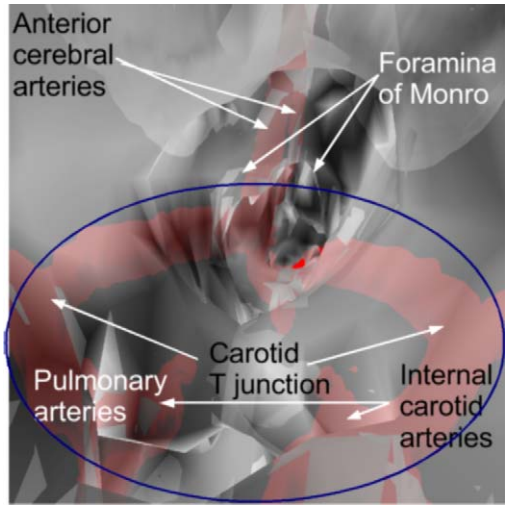

Fig. 11. Multimodal representation of cerebral ventricular system (3rd ventricle) and local vascular architecture from two registered MRI datasets, from an endoscopic point of view. The blue ellipsoid indicates the arterial circle of Willis near the base of the skull, where left and right internal carotid arteries branch to the middle and anterior cerebral arteries. This area indicates the target for certain endoscope interventions to treat a hydrocephalus (ventriculostomy), where a new drain of the ventricular system is realized.

Overall, HMDs are not well accepted in a clinical environment, which is mostly due to the limited optical possibilities (field of view, resolution) and the ergonomic deficiencies of wearing obstructing eye glasses or even more cumbersome helmets. The tracked semi-transparent MEDARPA display [73] is mounted on a swivel arm, and it is moved over the intervention site, where reality is seen through the display, and virtuality is displayed on the display. It provides good hand–eye coordination, similar to a HMD, but does not require a display immediately in front of the eyes. However, the attenuation due to the semi-transparency of the display reduces the brightness and contrast, and hence significantly reduces visibility. A standard display used by Fischer et al. [74] provides a good visual representation, but not a good hand–eye coordination, since the display is not positioned between the eyes of the surgeon and the intervention site. However, this system is designed for endoscopic representations, where the physician is used to look at a display instead of at the immediate intervention site. A different projection-only concept was proposed by Hoppe et al. [75] and later by Ritter et al. [76] where the virtual information is projected directly onto the organ during open surgery. However, the organ surface is not well suited as a projection screen; hence the visual quality remains quite low. In the following, we limit ourselves to video see-through, but the issues and solutions are similar for optical see-through. A survey on this discussion can be found in Azuma [77].

In order to combine the reality captured by the video camera and the virtuality, tracked by the tracking system, the video camera must be calibrated or registered to the tracking system, so that the video stream can be aligned with the patient dataset (extrinsic calibration). Typically, a specific pattern is used, which can be identified by the video software, like the video tracing system ARToolkit [78]. If the pattern is also registered/calibrated to the tracking system, the video image of the camera can be matched with the virtual information tracked by the tracking system. If the video camera is moved during the intervention, we also need to attach tracking markers of the tracking system to the camera body, so that the movement of the video camera can be tracked. Furthermore, if a video camera with non-standard optics is used, the optical system must be calibrated (intrinsic calibration) [79]. In an OR setting, additional tracking systems are not practical due to the additional setup costs. If a data interface to download the current tracking data is provided, this system can be used as tracking system [74].

A different issue of the use of mixed or augmented reality for medical applications is the depth perception. Johnson et al. [80] pointed out the problem of correct depth perception for transparent surface rendering in stereoscopic mixed reality of the optical see-through MAGI system [81]. A more recent discussion of this issue using different rendering alternatives was also provided by Sielhorst et al. [82]. Correct depth perception depends on many depth cues, such as motion parallax, relative size, perceptive distortions, illumination, shading, and occlusion. Even if a correct registration of the virtual information is provided, incorrect cues may seriously disturb the correct depth perception. One important cue is occlusion; if a virtual object that is located behind a real object is rendered on top of it, the depth perception is affected. Occlusion was one of the depth cues that was violated in the application examined by Johnson et al. [80]. The issue was aggravated by the use of transparent surfaces, which are known to reduce correct depth perception [83]. Solutions for the occlusion problem are discussed in the next section. A more detailed discussion of the role of perception for computer graphics can be found in a recent state-of-the-art report [84].

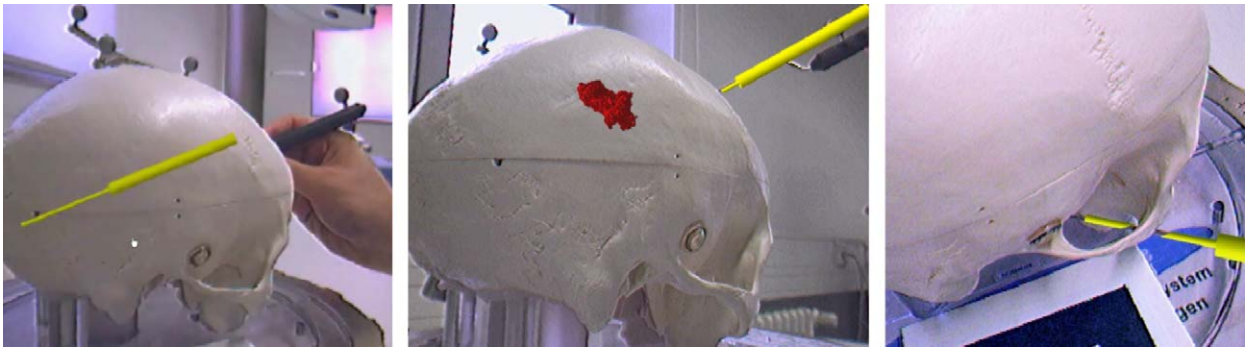

Fig. 12. Mixed reality display for a patient skull phantom without and with correct occlusion of reality. Left: the pointer tool vanishes behind the skull model, but its virtual representation is still rendered in front of the skull. Middle: a virtual representation of a tumor (red) is augmented in the camera image without considering occlusion. The virtual representation of the instrument (yellow) is augmented taking into account occlusion information. Right: the occlusion information is correctly computed also for complex situations, where the cheek bone occludes the instrument. Images are courtesy of Jan Fischer, University of Tubingen.

Approaches in a less clinical, more technical environment are described for ultrasound guided needle biopsy in classic papers of Bajura et al. [85] and State et al. [86]. Specifically mixed reality systems for liver surgery are discussed in Scheuering et al. [87], Olbrich et al. [88], and Lange et al. [89], and mixed reality endoscopy systems in Dey et al. [90]. Other approaches suggested another mixed reality endoscope system for the port placement for a surgical telemanipulator system [91] and a mixed reality microscope [81].

4.4. Occlusion handling

A different issue of mixed reality is known as the occlusion problem. This problem is based on the 3D nature of virtual objects and the lack of 3D information in the camera video stream. 3D objects can only be drawn over the camera video stream, resulting in incorrect depth sorting of 3D objects in the mixed stream. If the virtual object moves behind a real object in the camera stream, it will still be drawn on top of it, disturbing the immersion of the user (Fig. 12, left).

Different approaches have been proposed to address this problem. Breen et al. suggested the manual creation of geometric models of real scene objects to generate the missing 3D information [92]. This geometry is then used as phantom geometry to set the depth buffer for the subsequent rendering of the virtual objects. While this approach works quite well in static scenes, it involves a massive modeling effort for complex environments. This approach was later extended for the occlusion handling of an avatar representing a user [93]. More recently, a scenario for medical mixed reality has been described, in which the patient phantom geometry was extracted from volumetric datasets of the patients measured by a CT or MRI scan [94]. In this case, however, the high complexity of 3D models extracted from a volume dataset requires the simplification of the models to enable the mandatory interactive performance. This reduction can be achieved by extracting only a visual hull of the patient's geometry and removing all interior parts (Fig. 12 middle/right).

The phantom approach works well when sufficient information can be extracted for the occluding objects. In other cases, the information has to be extracted online from the video stream. Malik et al. [95] extracted the information by tracking planar features to estimate the hand of a user in a mixed reality environment. Dynamic occlusion with static backgrounds on the basis of textures for the background objects was addressed by Fischer et al. [96]. Finally, Berger [97] and Lepetit et al. [98] examined occlusion in stored video sequences.

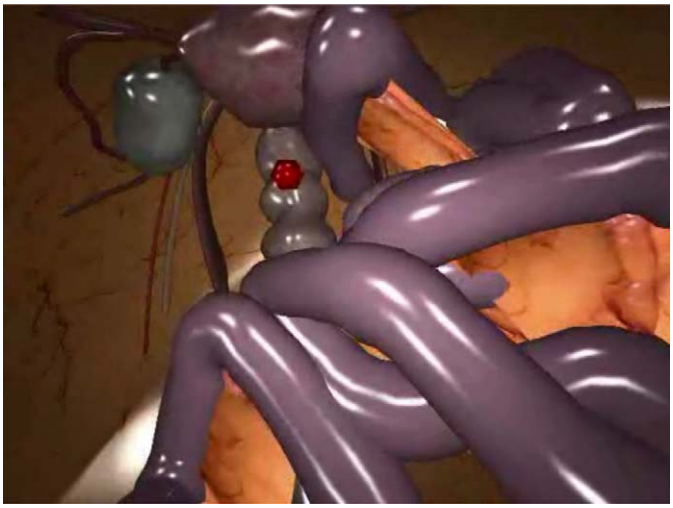

Fig. 13. Example application of collision detection (intestine surgery simulation). The objects in this case are highly deformable. Both self-collisions and collisions between different objects must be detected and handled. (Screenshot courtesy L. Raghupathi, L. Grisoni, F. Faure, D. Marchall, M.-P. Cani, C. Chaillou [99].)

4.5. Collision detection

Collision detection is an essential component in virtual and mixed reality applications (Fig. 13). In such environments, collisions between deformable organs have to be detected and handled. Furthermore, collisions between surgical tools and deformable tissue have to be processed and topological changes due to cutting may occur [100].

There are several different approaches to the collision detection process. Bounding volume hierarchies (BVHs) have proven to be very efficient for rigid objects [101,102]. A bounding volume hierarchy covering and partitioning an object is simply a tree where each node is associated with a bounding volume. BVHs can also be used when dealing with reduced deformable models [103].

In contrast to the object-partitioning methods, space-partitioning approaches are mainly used when objects are deformable as they are independent of changes in the object topology. For the partitioning, octrees [104], BSP trees [105] and voxel grids [106] have been proposed.

For scenarios where deformable objects have to be tested against rigid objects, e.g., between a surgical knife and a liver, distance fields are a very elegant and simple solution that also provides collision information like contact normals or penetration depths [107]. A distance field specifies the minimum distance to a

surface for all points in the field. In the literature, different data structures have been proposed for representing distance fields, e.g., octrees, BSP trees, or uniform grids. The problem of uniform grids, the large memory consumption, can be alleviated by a hierarchical data structure called adaptively sampled distance fields [108]. For the collision detection problem, special attention has to be paid to the continuity between different levels of the tree [109].

Stochastic methods are very interesting for time-critical scenarios. They offer the possibility to balance the quality of the collision detection against computation time, e.g., by selecting random pairs of colliding features as a guess of the potentially intersecting regions [110]. To identify the colliding regions when objects move or deform, temporal as well as spatial coherence can be exploited [111]. A stochastic approach can be applied to several collision detection problems [112].

Hardware-assisted approaches, especially full GPU implementations, have already been utilized for collision detection [113] and self-collision detection [114].

All mentioned collision detection algorithms provide some solutions for collision detection in medical applications. However, a best-suited approach for all situations does not exist. If collisions between rigid and deformable objects have to be tested, as in the case of intra-operative situations, distance fields may be very useful. In applications where a real-time response is most important, such as training simulations and other virtual reality applications, stochastic approaches or GPU-based implementations could be preferable, which may incur some occasional inaccuracies. If accuracy is of importance, then BVH-based approaches are probably the most suitable choice.

Current challenges in collision detection are

- deformable objects because it is notoriously difficult to find any acceleration data structures that can be updated quickly enough to be of any benefit;
- theoretical results about the average running time of the algorithms which may be very interesting for real-time scenarios;
- stochastic collision detection is still an area that has received very little attention; and
- collision detection on the recent multi-core architectures, such as the cell processor or NVidia's Tesla architecture.

5. Conclusions

We have reviewed several algorithms for processing and visualizing medical image data, including scalar, vector and tensor data, with the aim of supporting image-guided surgery and mixed-reality simulations. The challenge when developing such algorithms is to extract relevant information and to present it in perceptible way, preferably at interactive speed. Recent advances in volume rendering techniques, like interactive rendering of perspective projections, GPU-based ray-casting or semantic transfer functions, are able to handle the current sizes of medical data volumes and to present them to the clinician in an intuitive and useful way. However, interactive performance remains a problem.

Upcoming challenges include the visualization of multi-valued data. For example, clinical studies where patients are frequently examined with different medical imaging modalities are an important research area. There, multi-modal visualization techniques are used for merging relevant information. Moreover, vector valued and tensor valued data are gaining importance in the clinical environment.

An example is the diffusion weighted MRI modality for which visualization of glyphs, fiber tracking and clustering are some of the processing techniques considered in this work. As we mentioned, not much information can be extracted directly from the DTI raw data. Therefore, it is very important that image analysis and visualization techniques that help to understand these data are reliable. Furthermore, presenting the DTI data to a user in a comprehensive way where there is a balance between data simplification and clarity of the visualization remains an important issue.

In the context of vessel visualization, current challenges include the generation of geometric models appropriate for blood flow simulations. Latest results indicate that existing vessel visualization techniques may be adapted to produce meshes with sufficient triangle quality [115]. However, thorough investigations and comparisons with other techniques are necessary to come up with a reliable approach for visualizing vascular structures and simulating blood flow. With the information obtained via simulations, quantities such as wall shear stress which depend on morphologic, functional and dynamic factors may be investigated and visualized.

Finally, bringing the visualization algorithms from the research lab into the clinic and the operation room is not only an engineering task. In a lot of applications physicians or radiologists want to distinguish between healthy and pathology, or evaluate changes on time, in an objective way. Finding good quantitative non-biased ways to evaluate differences, as well as, visualization and navigation tools that help identify these differences is also of major importance for the clinical application of algorithms for medical diagnosis and treatment. Augmented- and mixed-reality methods are still at their inception state and collision detection algorithms must be developed so that no bottlenecks arise when utilizing them in mixed-reality simulations.

References

[1] Wigström L, Ebbers T, Fyrenius A, Karlsson M, Engvall J, Wranne B, et al. Particle trace visualization of intracardiac flow using time-resolved 3D phase contrast MRI. Magnetic Resonance in Medicine 1999;41(4):793–9.
[2] Basser P, Mattiello J, Bihan DL. MR diffusion tensor spectroscopy and imaging. Biophysical Journal 1994;66:259–67.
[3] Bartz D. Virtual endoscopy in research and clinical practice. Computer Graphics Forum 2005;24(1):111–26.
[4] Wolfsberger S, Neubauer A, Bühler K, Wegenkittl R, Czech T, Gentzsch S, et al. Advanced virtual endoscopy for endoscopic transsphenoidal pituitary surgery. Neurosurgery 2006;59(5):1001–9.
[5] Rezk-Salama C, Keller M, Kohlmann P. High-level user interfaces for transfer function design with semantics. In: Proceedings of IEEE visualization; 2006. p. 1021–8.
[6] Engel K, Hadwiger M, Kniss J, Rezk-Salama C, Kniss J. Real-time volume graphics. A K Peters, Ltd.; 2006.
[7] Krüger J, Westermann R. Acceleration techniques for GPU-based volume rendering. In: Proceedings of IEEE visualization; 2003. p. 287–92.
[8] Stegmaier S, Strengert M, Klein T, Ertl T. A simple and flexible volume rendering framework for graphics-hardware-based raycasting. In: Proceedings of volume graphics 2005; 2005. p. 187–95.
[9] Scharsach H, Hadwiger M, Neubauer A, Bühler K. Perspective isosurface and direct volume rendering for virtual endoscopy applications. In: Proceedings of Eurovis/IEEE-VGTC symposium on visualization; 2006. p. 315–22.
[10] Gobbetti E, Marton F, Iglesias Guitián J. A single-pass GPU ray casting framework for interactive out-of-core rendering of massive volumetric datasets. The Visual Computer 2008;24(7–9):797–806.
[11] Rezk-Salama C, Engel K, Bauer M, Greiner G, Ertl T. Interactive volume rendering on standard PC graphics hardware using multi-textures and multi-stage rasterization. In: Proceedings of SIGGRAPH/EG workshop on graphics hardware; 2000. p. 109–18.
[12] Grimm S, Bruckner S, Kanitsar A, Gröller E. Memory efficient acceleration structures and techniques for CPU-based volume raycasting of large data. In: Proceedings of IEEE/SIGGRAPH symposium on volume visualization and graphics; 2004. p. 1–8.
[13] Pfister H, Hardenbergh J, Knittel J, Lauer H, Seiler L. The VolumePro real-time ray-casting system. In: Proceedings of ACM SIGGRAPH; 1999. p. 251–60.
[14] Mroz L, Hauser H. RTVR: a flexible java library for interactive volume rendering. In: Proceedings of IEEE visualization; 2001. p. 279–86.

[15] Neophytou N, Mueller K. GPU accelerated image aligned splatting. In: Proceedings of volume graphics 2005; 2005. p. 197–205.
[16] Vega-Higuera F, Hastreiter P, Fahlbusch R, Greiner G. High performance volume splatting for visualization of neurovascular data. In: Proceedings of IEEE visualization; 2005. p. 271–8.
[17] Kniss J, McCormick P, McPherson A, Ahrens J, Painter J, Keahey A, et al. Interactive texture-based volume rendering for large data sets. IEEE Computer Graphics and Applications 2001;21(4):52–61.
[18] Hadwiger M, Sigg C, Scharsach H, Bühler K, Gross M. Real-time ray-casting and advanced shading of discrete isosurfaces. Computer Graphics Forum 2005;24(3):303–12.
[19] Ljung P, Winskog C, Persson A, Lundström C, Ynnerman A. Full body virtual autopsies using a state-of-the-art volume rendering pipeline. In: Proceedings of IEEE visualization; 2006. p. 869–76.
[20] Röttger S, Guthe S, Weiskopf D, Ertl T, Strasser W. Smart hardware-accelerated volume rendering. In: Proceedings of VisSym 2003; 2003. p. 231–8.
[21] Neubauer A, Wolfsberger S, Forster M-T, Mroz L, Wegenkittl R, Bühler K. Advanced virtual endoscopic pituitary surgery. IEEE Transactions on Visualization and Computer Graphics 2005;11(5):497–507.
[22] Kniss J, Kindlmann G, Hansen C. Interactive volume rendering using multi-dimensional transfer functions and direct manipulation widgets. In: Proceedings of IEEE visualization; 2001. p. 255–62.
[23] Kniss J, Premoze S, Ikits M, Lefohn A, Hansen C, Praun E. Gaussian transfer functions for multi-field volume visualization. In: Proceedings of IEEE visualization; 2003. p. 497–504.
[24] Rautek P, Bruckner S, Gröller ME. Semantic layers for illustrative volume rendering. In: Proceedings of IEEE visualization; 2007. p. 1336–43.
[25] Lundström C, Ljung P, Persson A, Ynnerman A. Uncertainty visualization in medical volume rendering using probabilistic animation. In: Proceedings of IEEE visualization; 2007. p. 1648–55.
[26] Johnson CR, Moorhead R, Munzner T, Pfister H, Rheingans P, Yoo TS. NIH-NSF visualization research challenges report. Los Alamitos, CA, USA: IEEE Press; 2006.
[27] Hadwiger M, Berger C, Hauser H. High-quality two-level volume rendering of segmented data sets on consumer graphics hardware. In: Proceedings of IEEE visualization; 2003. p. 301–8.
[28] Beyer J, Hadwiger M, Wolfsberger S, Bühler K. High-quality multimodal volume rendering for preoperative planning of neurosurgical interventions. In: Proceedings of IEEE visualization; 2007. p. 1696–703.
[29] Kniss J, Van Uitert R, Stephens A, Li G-S, Tasdizen T, Hansen C. Statistically quantitative volume visualization. In: Proceedings of IEEE visualization; 2005. p. 287–94.
[30] Rezk-Salama C, Kolb A. Opacity peeling for direct volume rendering. Computer Graphics Forum 2006:597–606.
[31] Horsfield M, Jones D. Applications of diffusion-weighted and diffusion tensor MRI to white matter diseases—a review. Nuclear Magnetic Resonance in Biomedicine 2002;15(7–8):570–7.
[32] Sundgren P, Dong Q, Gomez-Hassan D, Mukherji S, Maly P, Welsh R. Diffusion tensor imaging of the brain: review of clinical applications. Neuroradiology 2004;46(5):339–50.
[33] Peeters T, Vilanova A, Strijkers G, Haar Romeny Bt. Visualization of the fibrous structure of the heart. In: Proceedings of vision modeling and visualization; 2006. p. 309–17.
[34] Pul C, Buijs J, Vilanova A, Roos F, Wijn P. Fiber tracking in newborns with perinatal hypoxic-ischemia at birth and at 3 months. Radiology 2006; 240(1):203–14.
[35] Basser P, Pierpaoli C. Microstructural features measured using diffusion tensor imaging. Journal of Magnetic Resonance 1996:209–19.
[36] Kindlmann G, Weinstein D, Hart D. Strategies for direct volume rendering of diffusion tensor fields. IEEE Transactions on Visualization and Computer Graphics 2000;6(2):124–38.
[37] Kindlmann G. Superquadric tensor glyphs. In: Data visualization (Proceedings of Eurographics/IEEE symposium on visualization); 2004. p. 147–54.
[38] Kindlmann G, Westin C-F. Diffusion tensor visualization with glyph packing. IEEE Transactions on Visualization and Computer Graphics 2006;12(5): 1329–36.
[39] Basser P, Pajevic S, Pierpaoli C, Duda J, Aldroubi A. In vivo fiber tractography using DT-MRI data. Magnetic Resonance in Medicine 2000;44(4):625–32.
[40] Mori S, Zijl Pv. Fiber tracking: principles and strategies—a technical review. Nuclear Magnetic Resonance in Biomedicine 2002;15(7–8):468–80.
[41] Weinstein D, Kindlmann G, Lundberg E. Tensorlines: advection–diffusion based propagation through diffusion tensor fields. In: Proceedings of IEEE visualization; 1999. p. 249–53.
[42] Zhang S, Demiralp C, Laidlaw D. Visualizing diffusion tensor MR images using streamtubes and streamsurfaces. IEEE Transactions on Visualization and Computer Graphics 2003;9(4):454–62.
[43] Vilanova A, Berenschot G, Pul Cv. DTI visualization with streamsurfaces and evenly-spaced volume seeding. In: Data visualization (Proceedings of Eurographics/IEEE symposium on visualization), Eurographics Association; 2004. p. 173–82.
[44] Brun A, Björnemo M, Kikinis R, Westin C-F. White matter tractography using sequential importance sampling. In: Proceeding of ISMRM; 2002. p. 1131.
[45] Lua Y, Aldroubib A, Gorea JC, Andersona A, Dinga Z. Improved fiber tractography with Bayesian tensor regularization. NeuroImage 2006;31(3): 1061–74.
[46] Friman O, Farneback G, Westin C-F. A Bayesian approach for stochastic white matter tractography. IEEE Transactions on Medical Imaging 2006;25(8): 965–78.
[47] Brun A, Knutsson H, Park HJ, Shenton ME, Westin C-F. Clustering fiber tracts using normalized cuts. In: Proceedings of medical image computing and computer-assisted intervention (MICCAI); 2004. p. 368–75.
[48] Klein J, Bittihn P, Ledochowitsch P, Hahn HK, Konrad O, Rexilius J, Peitgen H-O. Grid-based spectral fiber clustering. In: Proceedings of SPIE medical imaging, vol. 6509, 2007. p. 65091E-1–65091E-10.
[49] Moberts B, Vilanova A, van Wijk J. Evaluation of fiber clustering methods for diffusion tensor imaging. In: Proceedings of IEEE visualization; 2005. p. 65–72.
[50] Ritter F, Hansen C, Dicken V, Konrad O, Preim B, Peitgen H-O. Real-time illustration of vascular structures. In: Proceedings of IEEE visualization, vol. 12(5), 2006. p. 877–84.
[51] Tomandl BF, Köstner NC, Schempershofe M, Huk WJ, Strauss C, Anker L, et al. CT angiography of intracranial aneurysms: a focus on postprocessing. Radiographics 2004;24(3):637–55.
[52] Glaßer S, Oeltze S, Hennemuth A, Kubisch C, Mahnken A, Wilhelmsen S, Preim B. Automatic transfer function specification for visual emphasis of coronary artery plaque. Technical Report no. FIN-006-2009, Otto-von-Guericke University, Magdeburg (http://www.cs.uni-magdeburg.de/fin_media/downloads/forschung/preprints/2009/TechReport06.pdf).
[53] Boskamp T, Hahn H, Hindennach M, Zidowitz S, Oeltze S, Preim B, et al. Geometrical and structural analysis of vessel systems in 3D medical image datasets. Medical Imaging Systems Technology 2005;5:1–60.
[54] Masutani Y, Masamune K, Dohi T. Region-growing-based feature extraction algorithm for tree-like objects. Visualization in Biomedical Computing 1996;1131:161–71.
[55] Hahn HK, Preim B, Selle D, Peitgen H-O. Visualization and interaction techniques for the exploration of vascular structures. In: Proceedings of IEEE visualization; 2001. p. 395–402.
[56] Ehricke H, Donner K, Killer W, Straßer W. Visualization of vasculature from volume data. Computers and Graphics 1994;18(3):395–406.
[57] Felkel P, Wegenkittl R, Bühler K. Surface models of tube trees. In: Computer graphics international; 2004. p. 70–7.
[58] Bloomenthal J, Shoemake K. Convolution surfaces. In: Proceedings of ACM SIGGRAPH; 1991. p. 251–6.
[59] Oeltze S, Preim B. Visualization of vascular structures with convolution surfaces: method, validation and evaluation. IEEE Transactions on Medical Imaging 2005;25(4):540–9.
[60] Bühler K, Felkel P, Cruz AL. Geometric methods for vessel visualization and quantification—a survey. In: Brunnet G, Hamann B, Müller H, editors. Geometric modeling for scientific visualization. Berlin: Springer; 2004. p. 399–420.
[61] Preim B, Bartz D. Visualization in medicine—theory, algorithms, and applications. Burlington: Morgan Kaufmann; 2007.
[62] Maintz J, Viergever M. A survey of medical image registration. Medical Image Analysis 1998;2(1):1–36.
[63] Kettenbach J, Kacher D, Koskinen S, Silverman S, Nabavi A, Gering D, et al. Interventional and intraoperative magnetic resonance imaging. Annual Review of Biomedical Engineering 2000;2:661–90.
[64] Nimsky C, Ganslandt O, von Keller B, Fahlbusch R. Preliminary experience in glioma surgery with intraoperative high-field MRI. Acta Neurochirurgica 2003;88:21–9.
[65] Sauer F, Khamene A, Bascle B, Schimmang L, Wenzel F, Vogt S. Augmented reality visualization of ultrasound images: system description, calibration, and feature. In: Proceedings of IEEE and ACM international workshop on augmented reality; 2001. p. 30.
[66] Lange T, Eulenstein S, Hünerbein M, Schlag P. Vessel-based non-rigid registration of MR/CT and 3D ultrasound for navigation in liver surgery. Computer Aided Surgery 2002;8(5):228–40.
[67] Khamene A, Vogt S, Azar F, Sielhorst T, Sauer F, Niemann H. Local 3D reconstruction and augmented reality visualization of free-hand ultrasound for needle biopsy procedures. In: Proceedings of medical image computing and computer-assisted intervention (MICCAI), Lecture notes in computer science; 2003. p. 344–55.
[68] Lindner D, Trantakis C, Arnold S, Schmitgen A, Schneider J, Meixensberger J. Neuronavigation based on intraoperative 3D-ultrasound during tumor resection. In: Proceedings of computer assisted radiology and surgery; 2005. p. 815–20.
[69] Navab N, Bani-Hashemi A, Mitschke M. Merging visible and invisible: two camera-augmented mobile C-arm (CAMC) applications. In: Proceedings of IEEE and ACM international workshop on augmented reality; 1999. p. 134–41.
[70] Binstadt E, Walls R, White B, Nadel E, Takayesu J, Barker T, et al. A comprehensive medical simulation education curriculum for emergency medicine residents. Annals of Emergency Medicine 2007;49(4):495–504.
[71] Birkfellner W, Figl M, Huber K, Watzinger F, Wanschitz F, Hanel R, et al. The varioscope AR—a head-mounted operating microscope for augmented reality. In: Proceedings of medical image computing and computer-assisted intervention (MICCAI), Lecture notes in computer science; 2000. p. 869–77.
[72] Vogt S, Khamene A, Sauer F, Keil A, Niemann H. Single camera tracking of marker clusters: multiparameter cluster optimization and experimental verification. In: Proceedings of IEEE and ACM international symposium on mixed and augmented reality; 2002. p. 127–36.

[73] Schwald B, Seibert H, Weller T. A flexible tracking concept applied to medical scenarios using an AR window. In: Proceedings of IEEE and ACM international symposium on mixed and augmented reality; 2002. p. 261–2.
[74] Fischer J, Neff M, Bartz D, Freudenstein D. Medical augmented reality based on commercial image guided surgery. In: Proceedings of Eurographics symposium on virtual environments; 2004. p. 83–6.
[75] Hoppe H, Däuber S, Raczkowsky J, Wörn H, Moctezuma J. Intraoperative visualization of surgical planning data using video projectors. In: Proceedings of medicine meets virtual reality; 2001. p. 206–8.
[76] Ritter F, Hansen C, Dicken V, Konrad-Verse O, Preim B, Peitgen H-O. Real-time illustration of vascular structures. IEEE Transactions on Visualization and Computer Graphics 2006;12(5):877–84.
[77] Azuma R. A survey of augmented reality. Presence: Teleoperators and Virtual Environments 1997;6(4):355–85.
[78] Kato H, Billinghurst M. Marker tracking and HMD calibration for a video-based augmented reality conferencing system. In: Proceedings of IEEE and ACM international workshop on augmented reality; 1999. p. 85–94.
[79] Kannala J, Brandt S. A generic camera model and calibration method for conventional wide-angle and fish-eye lenses. IEEE Transactions on Pattern Analysis and Machine Intelligence 2006;28(8):1335–40.
[80] Johnson L, Edwards P, Hawkes D. Surface transparency makes stereo overlays unpredictable: the implications for augmented reality. In: Proceedings of medicine meets virtual reality; 2003. p. 131–6.
[81] Edwards P, King A, Maurer C, de Cunha D, Hawkes D, Hill D, et al. Design and evaluation of a system for microscope-assisted guided interventions (MAGI). In: Proceedings of medical image computing and computer-assisted intervention (MICCAI), Lecture notes in computer science; 1999. p. 842–51.
[82] Sielhorst T, Bichlmeier C, Heining S, Navab N. Depth perception—a major issue in medical AR: evaluation study by twenty surgeons. In: Proceedings of medical image computing and computer-assisted intervention (MICCAI), Lecture notes in computer science; 2006. p. 364–72.
[83] Bair A, House D. A grid with a view: optimal texturing for perception of layered surface shape. In: Proceedings of IEEE visualization; 2007. p. 1656–63.
[84] Bartz D, Cunningham D, Fischer J, Wallraven C. The role of perception for computer graphics. In: Eurographics state-of-the-art-reports; 2008. p. 65–86.
[85] Bajura M, Fuchs H, Ohbuchi R. Merging virtual objects with the real world: seeing ultrasound imaginery within the patient. In: Proceedings of ACM SIGGRAPH; 1992. p. 203–10.
[86] State A, Livingston M, Hirota G, Garrett W, Whitton M, Fuchs H, et al. Technologies for augmented-reality systems: realizing ultrasound-guided needle biopsies. In: Proceedings of ACM SIGGRAPH; 1996. p. 439–46.
[87] Scheuering M, Schenk A, Schneider A, Preim B, Greiner G. Intra-operative augmented reality for minimally invasive liver interventions. In: Proceedings of SPIE medical imaging; 2003. p. 407–17.
[88] Olbrich B, Traub J, Wiesner S, Wichert A, Feußner H, Navab N. Respiratory motion analysis: towards gated augmentation of the liver. In: Proceedings of computer assisted radiology and surgery; 2005. p. 248–53.
[89] Lange T, Eulenstein S, Hünerbein M, Lamecker H, Schlag P. Augmenting intraoperative 3D ultrasound with preoperative models for navigation in liver surgery. In: Proceedings of medical image computing and computer-assisted intervention (MICCAI), Lecture notes in computer science, vol. 3217; 2004. p. 534–41.
[90] Dey D, Slomka P, Gobbi D, Peters T. Mixed reality merging of endoscopic images and 3D surfaces. In: Proceedings of medical image computing and computer-assisted intervention (MICCAI), Lecture notes in computer science; 2000. p. 796–803.
[91] Feuerstein M, Wildhirt SM, Bauernschmitt R, Navab N. Automatic patient registration for port placement in minimally invasive endoscopic surgery. In: Proceedings of medical image computing and computer-assisted intervention (MICCAI), Lecture notes in computer science; 2005. p. 287–94.
[92] Breen D, Whitaker R, Rose E, Tuceryan M. Interactive occlusion and automatic object placement for augmented reality. Computer Graphics Forum 1996;15(3):11–22.
[93] Fuhrmann A, Hesina G, Faure F, Gervautz M. Occlusion in collaborative augmented environments. Computers & Graphics 1999;23(6):809–19.
[94] Fischer J, Bartz D, Straßer W. Occlusion handling for medical augmented reality using a volumetric phantom model. In: Proceedings of ACM symposium on virtual reality software and technology; 2004. p. 174–7.
[95] Malik S, McDonald C, Roth G. Hand tracking for interactive pattern-based augmented reality. In: Proceedings of IEEE and ACM international symposium on mixed and augmented reality; 2002. p. 117–26.
[96] Fischer J, Regenbrecht H, Baratoff G. Detecting dynamic occlusion in front of static backgrounds for AR scenes. In: Proceedings of Eurographics symposium on virtual environments; 2003. p. 153–61.
[97] Berger M. Resolving occlusion in augmented reality: a contour based approach without 3D reconstruction. In: Proceedings of the IEEE conference on computer vision and pattern recognition; 1997. p. 91–6.
[98] Lepetit V, Berger M. A semi-automatic method for resolving occlusion in augmented reality. In: Proceedings of the IEEE conference on computer vision and pattern recognition; 2000. p. 2225–30.
[99] Raghupathi L, Grisoni L, Faure F, Marchall D, Cani M-P, Chaillou C. An intestine surgery simulator: real-time collision processing and visualization. IEEE Transactions on Visualization and Computer Graphics (TVCG) 2004; 10(6):708–18.
[100] Teschner M, Kimmerle S, Heidelberger B, Zachmann G, Raghupathi L, Fuhrmann A, et al. Collision detection for deformable objects. Computer Graphics forum 2005;24(1):61–81.
[101] Gottschalk S, Lin M, Manocha D. OBB-tree: a hierarchical structure for rapid interference detection. Proceedings of ACM SIGGRAPH 1996;15(3):171–80.
[102] Klosowski JT, Held M, Mitchell JSB, Sowrizal H, Zikan K. Efficient collision detection using bounding volume hierarchies of *k*-DOPs. IEEE Transactions on Visualization and Computer Graphics 1998;4(1):21–36.
[103] James DL, Pai DK. BD-tree: output-sensitive collision detection for reduced deformable models. Proceedings of ACM SIGGRAPH 2004;23(3):393–8.
[104] Bandi S, Thalmann D. An adaptive spatial subdivision of the object space for fast collision detection of animating rigid bodies. Computer Graphics Forum 1995;14(3):259–70.
[105] Melax S. Dynamic plane shifting BSP traversal. In: Graphics interface 2000; 2000. p. 213–20.
[106] McNeely WA, Puterbaugh KD, Troy JJ. Six degrees-of-freedom haptic rendering using voxel sampling. In: Proceedings of ACM SIGGRAPH, vol. 18(3), 1999. p. 401–8.
[107] Sigg C, Peikert R, Gross M. Signed distance transform using graphics hardware. In: IEEE Vis2003; 2003. p. 83–90.
[108] Frisken SP, Perry RN, Rockwood AP, Jones TR. Adaptively sampled distance fields: a general representation of shape for computer graphics. In: Proceedings of ACM SIGGRAPH, vol. 19(3), 2000. p. 249–54.
[109] Bridson R, Marino S, Fedkiw R. Simulation of clothing with folds and wrinkles. In: Proceedings of ACM SIGGRAPH/Eurographics symposium on computer animation (SCA '03), Eurographics Association; 2003. p. 28–36.
[110] Raghupathi L, Cantin V, Faure F, Cani M-P. Real-time simulation of self-collisions for virtual intestinal surgery. In: Ayache N, Delingette H, editors. Proceedings of international symposium on surgery simulation and soft tissue modeling, Lecture notes in computer science, vol. 2673. Berlin: Springer; 2003. p. 15–26.
[111] Lin MC, Canny JF. Efficient collision detection for animation. In: Proceedings of 3rd Eurographics workshop on animation and simulation, Cambridge, England; 1992.
[112] Debunne G, Desbrun M, Cani M-P, Barr AH. Dynamic real-time deformations using space and time adaptive sampling. In: Proceedings of ACM SIGGRAPH, vol. 20(3), 2001. p. 31–6.
[113] Govindaraju N, Lin M, Manocha D. Fast and reliable collision culling using graphics hardware. IEEE Transactions on Visualization and Computer Graphics 2006;12(2):143–54.
[114] Baciu G, Wong WS-K. Hardware-assisted self-collision for deformable surfaces. In: Proceedings of ACM symposium on virtual reality software and technology (VRST 2002), Hong Kong, China; 2002. p. 129–36.
[115] Schumann C, Neugebauer M, Bade R, Peitgen H-O, Preim B. Implicit vessel surface reconstruction for visualization and CFD simulation. International Journal of Computer Assisted Radiology and Surgery 2008;2(5):275–86.